

Transportation of homogeneous–heterogeneous reactions in flow of Sutterby fluid confined between two co-axially rotating disks

M Ijaz Khan^{1,3} , M Waleed Ahmad Khan¹, Salman Ahmad^{1,3} ,
T Hayat^{1,2} and A Alsaedi²

¹Department of Mathematics, Quaid-I-Azam University, Islamabad 44000, Pakistan

²Nonlinear Analysis and Applied Mathematics (NAAM) Research Group, Department of Mathematics, Faculty of Science, King Abdulaziz University, PO Box 80257, Jeddah 21589, Saudi Arabia

E-mail: mikhan@math.qau.edu.pk and salmanuom206@gmail.com

Received 24 April 2019, revised 5 September 2019

Accepted for publication 19 September 2019

Published 25 February 2020



Abstract

In this paper we investigated the homogeneous–heterogeneous reactions in flow of Sutterby fluid. Flow is considered between two infinite parallel rotating stretchable disks. Effects of magnetohydrodynamic, heat source/sink, nonlinear mixed convection and radiative heat flux are considered. Suitable similarity transformations are utilized to convert the nonlinear partial differential equations into ordinary ones. The obtained system of equations is tackled numerically through Shooting technique. Impacts of pertinent flow variables on velocity, mass concentration and temperature are described graphically in detail. Skin friction (surface drag force) and heat transfer rate (Nusselt number) are numerically discussed and presented via tables. The obtained outcomes present that velocity of liquid particles decays with material and magnetic parameters. Temperature enhances through thermal radiation, heat generation and temperature ratio variables but it reduces through larger Reynolds number.

Keywords: Sutterby liquid, nonlinear mixed convection and thermal radiation, rotating stretchable disks, heat generation, homogeneous–heterogeneous reactions

(Some figures may appear in colour only in the online journal)

1. Introduction

Many scientists and researchers examined the fluid flow due to rotating disk broadly because of its numerous engineering and industrial applications. Such applications include medical equipment, rotating machinery, air cleaning machine, computer storage devices, food processing technology, electric power generating system, aero dynamical engineering, gas turbine rotors, crystal growth processes etc. Karman [1] firstly examined hydrodynamic flow subject to rotating disk. He developed appropriate transformations to transform governing PDEs into obtained system of equations. Flow behavior

between a porous stationary disk and a solid rotating disk is examined by Kumar *et al* [2]. Flow due to rotating disk with nanomaterials is examined by Turkyilmazoglu [3]. Viscoelastic nanomaterial convective flow inside two rotating stretchable disks is investigated by Hayat *et al* [4]. Sheikholeslami *et al* [5] scrutinized flow of nanomaterial by rotating inclined disk. Mass and heat transport in magnetohydrodynamic (MHD) flow of copper and silver water by a rotating disk is examined by Sudarsana *et al* [6]. They implemented broadly validated finite element technique. Their obtained outcomes show that velocity, temperature and concentration gradients strongly depend upon flow variable. Some studies exploring rotating disk flow can be seen in [6–10].

³ Authors to whom any correspondence should be addressed.

Homogeneous–heterogeneous reactions arise in chemical reaction processes. In homogeneous reaction the products and reactants are in the same phase while in heterogeneous reaction they are in different phase. Homogeneous–heterogeneous reactions occurring in catalysis, combustion, crops damaging through freezing, biochemical system, fog dispersion, cooling towers and hydrometallurgical procedures. Initially Merkin [11] proposed a model for the homogeneous–heterogeneous reactions in flow of Newtonian material over a plate. Khan and Pop [12] considered effect of homogeneous–heterogeneous reactions for two-dimensional stagnation point flow by permeable wall. They used finite difference method for solution and observed that characteristics of flow are considerably affected by mass transfer variable. Some valuable investigations on such types of flows are mentioned in [13–17].

Convective heat transport is essential for frequent industrial heating and cooling materials. Heat exchangers, chilling of electrical items, internal freshening with radiators, chilling of reactors etc, are some designs for such developments. Mixed/natural convection is an essential and fundamental area of heat transport in many applications. Beside these, the contemporaneous outgrowth of thermal radiation and forced/mixed convection are of fundamental importance in human body essentially in heart, liver, brain and in constriction of skeletal muscles. Radiative heat flux can control the super abundance of heat source/sink in the human body [17–23] present frequent studies about radiation/mixed convection.

In this work we have considered flow of homogeneous–heterogeneous reactions of Sutterby fluid confined between two coaxially stretchable disks. Furthermore, MHD, heat source/sink, nonlinear radiative heat flux and mixed convection are considered. The nonlinear ordinary system is numerically solved via Shooting technique. Some meaningful considerations about Newtonian and non-Newtonian fluid flows are listed in [24–60]. The influence of involved parameters on velocity, mass concentration and temperature are examined graphically. Velocity and temperature gradients (skin friction and Nusselt number) are calculated numerically through tables.

2. Constitutive expressions

For Sutterby fluid the extra stress tensor is mathematically addressed as

$$\boldsymbol{\tau} = -p\mathbf{I} + \mathbf{S}, \quad (1)$$

where

$$\mathbf{S} = \frac{\mu_0}{2} \left[\frac{\sinh^{-1}(\beta_1 \gamma)}{\beta_1 \gamma} \right]^n \tilde{\mathbf{A}}. \quad (2)$$

In the above equations

$$\tilde{\mathbf{A}} = (\text{grad } V) + (\text{grad } V)^T, \quad (3)$$

$$\gamma = \sqrt{\sum_i \sum_j \gamma_{i1} \gamma_{j1}} = \sqrt{\frac{\Lambda}{2}}, \quad (4)$$

$$\Lambda = \text{trace}[(\text{grad } V) + (\text{grad } V)^T]^2. \quad (5)$$

Here $\boldsymbol{\tau}$ denotes the Cauchy stress tensor, p the pressure, \mathbf{I} the identity tensor, \mathbf{S} the extra stress tensor, n and β_1 denote the material constants, $\tilde{\mathbf{A}}$ the first Rivlin Erickson tensor, μ_0 the viscosity at low shear rates, Λ the second invariant strain tensor and γ the shear rate. Through binomial expansion one has

$$\sinh^{-1}(\beta_1 \gamma) \cong \beta_1 \gamma - \frac{(\beta_1 \gamma)^3}{6}. \quad (6)$$

In case of Sutterby liquid, the viscosity relation is defined as

$$\mu = \mu_0 \left[\frac{\sinh^{-1}(\beta_1 \gamma)}{\beta_1 \gamma} \right]^n. \quad (7)$$

The second order approximation for viscosity relation after using equation (6) in (7) is given below:

$$\mu \cong \mu_0 \left[1 - \frac{(\beta_1 \gamma)^2}{6} \right]^n \cong \mu_0 \left[1 - \frac{n(\beta_1 \gamma)^2}{6} \right]. \quad (8)$$

For $n = 0, 1$ the model reduces to viscous fluid and Eyring model respectively. For $n = 0$, $\mu = \mu_0$ which is viscous fluid and for $n = 1$, equation (8) becomes $\mu \cong \mu_0 \left[1 - \frac{(\beta_1 \gamma)^2}{6} \right]$ which is Eyring model.

3. Statement

Here we have considered steady, incompressible (3D) flow of Sutterby fluid confined between two coaxially stretchable rotating disks. The lower disk placed at $z = 0$, is rotating and stretching with rates Ω_1 and c_1 respectively. Both the disks are placed at a distance h from each other. The upper disk is rotating and stretching with rates Ω_2 and c_2 . It is assumed that T_1 and T_2 are temperatures of lower and upper disk respectively. MHD fluid is considered. Magnetic field is applied in z -direction, therefore in z -direction the impact of magnetic field is zero. Mixed convection effect is further accounted. The flow is generated by rotating stretching surface of the disk. Isothermal and single chemical reaction i.e. homogeneous and heterogeneous reactions are considered. Energy equation is discussed in the presence of thermal radiative heat and heat source/sink. Fourier's law of heat conduction is used for the heat transport. At lower and upper disks, the temperatures are constant. It is also assumed that $u = rc_1$ and $v = \Omega_1 r$ and $u = rc_2$ and $v = \Omega_2 r$ are the stretching and angular velocities of both lower and upper disks respectively. The schematic flow diagram is presented in figure 1. The considered fluid model predict the shear thickening behavior for $n > 1$, and shear thinning behavior for $n < 1$. The considered fluid model reduces to Newtonian fluid for $n = 1$. Here we have discussed the fluid model only for shear thickening behavior i.e. $n = 1.5$. The homogeneous–heterogeneous reactions for the chemical species B^*

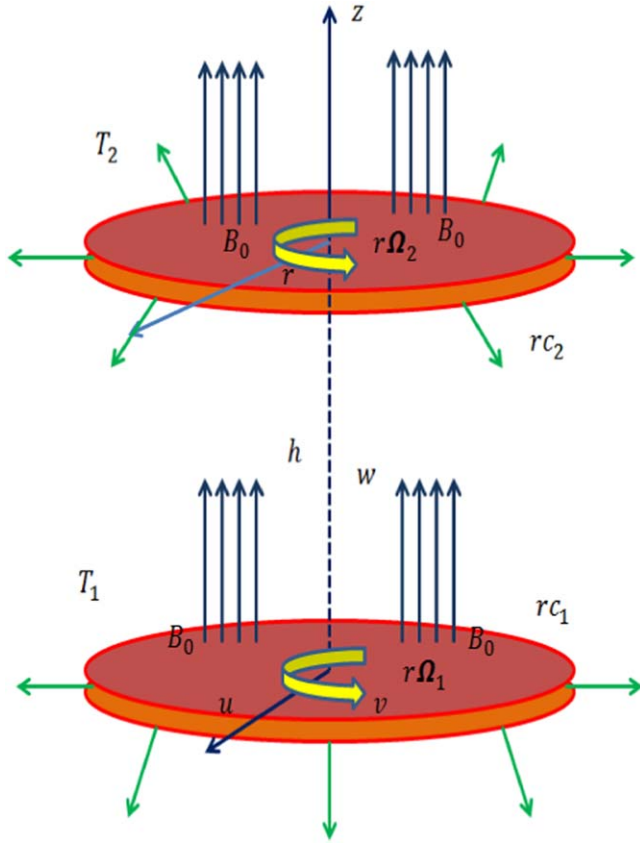
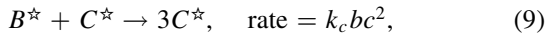
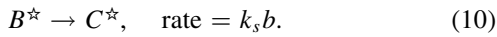


Figure 1. Systematic diagram of the problem.

and C^* [14] are defined as



on the surface, first order isothermal and single chemical reaction is defined as



In the above two equations b and c denote species of the reactants and k_c and k_s indicate the rate constants. Mathematically, the flow expressions in components form are addressed as

$$\frac{\partial u}{\partial r} + \frac{u}{r} + \frac{\partial w}{\partial z} = 0, \quad (11)$$

$$\left. \begin{aligned} \rho \left(u \frac{\partial u}{\partial r} + w \frac{\partial u}{\partial z} - \frac{v^2}{r} \right) &= \frac{2}{r} \frac{\partial}{\partial r} \left(r^2 \mu \frac{\partial u}{\partial r} \right) \\ &- 2 \frac{\mu u}{r^2} + \frac{\partial}{\partial z} \left(\mu \left(\frac{\partial u}{\partial z} + \frac{\partial w}{\partial r} \right) \right) \\ &- \delta B_0^2 u + \rho g \{ \alpha_1 (T - T_2) + \alpha_2 (T - T_2)^2 \}, \end{aligned} \right\} \quad (12)$$

$$\left. \begin{aligned} \rho \left(u \frac{\partial v}{\partial r} + w \frac{\partial v}{\partial z} + \frac{uv}{r} \right) &= \frac{1}{r^2} \left(r^2 \mu \left(\frac{\partial v}{\partial r} - \frac{v}{r} \right) \right) \\ &+ \frac{\partial}{\partial z} \left(\mu \frac{\partial v}{\partial z} \right) - \delta B_0^2 v, \end{aligned} \right\} \quad (13)$$

$$\left. \begin{aligned} \rho \left(u \frac{\partial w}{\partial r} + w \frac{\partial w}{\partial z} \right) &= \frac{1}{r} \frac{\partial}{\partial r} \left(r \mu \left(\frac{\partial u}{\partial z} + \frac{\partial w}{\partial r} \right) \right) \\ &+ 2 \frac{\partial}{\partial z} \left(\mu \frac{\partial w}{\partial z} \right) - \delta B_0^2 w, \end{aligned} \right\} \quad (14)$$

$$\left. \begin{aligned} u \frac{\partial T}{\partial r} + w \frac{\partial T}{\partial z} &= \frac{k}{\rho c_p} \left(u \frac{\partial^2 T}{\partial r^2} + \frac{1}{r} \frac{\partial T}{\partial r} + \frac{\partial^2 T}{\partial z^2} \right) \\ &- \frac{1}{\rho c_p} \frac{\partial q_z}{\partial z} + \frac{Q_0}{\rho c_p} (T - T_\infty), \end{aligned} \right\} \quad (15)$$

$$u \frac{\partial b}{\partial r} + w \frac{\partial b}{\partial z} = D_B \left(\frac{\partial^2 b}{\partial z^2} + \frac{1}{r} \frac{\partial b}{\partial r} + \frac{\partial^2 b}{\partial r^2} \right) - k_c bc^2, \quad (16)$$

$$u \frac{\partial c}{\partial r} + w \frac{\partial c}{\partial z} = D_C \left(\frac{\partial^2 c}{\partial z^2} + \frac{1}{r} \frac{\partial c}{\partial r} + \frac{\partial^2 c}{\partial r^2} \right) + k_c bc^2, \quad (17)$$

$$\left. \begin{aligned} u &= rc_1, \quad v = \Omega_1 r, \quad w = 0, \quad T = T_1, \quad D_B \frac{\partial b}{\partial z} \\ &= k_s b, \quad D_C \frac{\partial c}{\partial z} = -k_s b \quad \text{at } z = 0 \\ u &= rc_2, \quad v = \Omega_2 r, \quad T = T_2, \quad b \rightarrow b_0, \\ c &\rightarrow 0, \quad \text{at } z = h, \end{aligned} \right\} \quad (18)$$

where u, v, w indicate the velocity components, r, θ, z the cylindrical coordinates, T the temperature, ρ density, μ dynamic viscosity, δ electric conductivity, c_p specific heat, B_0 magnetic field strength, Q_0 coefficient of heat source/sink, g gravity, q_z the radiative heat flux, T_1 and T_2 temperatures at disks, D_B and D_C diffusion coefficients and α_1 and α_2 linear and nonlinear thermal expansion coefficients.

Here we have applied Roseland approximation for describing radiative heat flux. Radiative heat flux is neglected in r -direction due to minimum effect in comparison with z -direction [61–63]. So radiative heat flux q_z mathematical expression is:

$$q_z = \frac{-4\delta^*}{3k^*} \frac{\partial(T^4)}{\partial z}, \quad (19)$$

where δ^* and k^* are Stefan–Boltzmann constant and mean absorption coefficient. We have taken the assumption that small temperature differences occurs only. So for this purpose we will define T^4 as linear function of temperature. By expanding T^4 in a Taylor series around T_2 we have:

$$T^4 = T_2^4 + 4T_2^3(T - T_2) + 6T_2^2(T - T_2)^2 + \dots \quad (20)$$

By neglecting the higher order terms of $(T - T_2)$ one can take the form

$$T^4 = 4T_2^3 T - 3T_2^4. \quad (21)$$

Now the component of radiative flux (q_z) is given by

$$q_z = -\frac{4\delta^*}{3k^*} \frac{\partial T^4}{\partial z} = -\frac{16\delta^* T^3}{3k^*} \frac{\partial T}{\partial z}. \quad (22)$$

Letting,

$$\left. \begin{aligned} u &= r\Omega_1 f'(\eta), \quad v = r\Omega_1 g(\eta), \quad w = -2h\Omega_1 f(\eta), \\ \theta(\eta) &= \frac{T - T_2}{T_1 - T_2}, \quad b = b_0 \phi, \quad c = b_0 \phi, \quad \eta = \frac{z}{h}. \end{aligned} \right\} \quad (23)$$

We have

$$\left. \begin{aligned} f''' - 2n\varepsilon^2[2f'f''^2 + f'^2f'''] \\ + Re[g^2 + 2ff'' - f'^2] \\ - MRe f' + Re\lambda_1(1 + \lambda_2\theta)\theta = 0, \end{aligned} \right\} \quad (24)$$

$$\begin{aligned} g'' - 2n\varepsilon^2[2f'f''g' + f'^2g''] - 2Re[f'g - fg'] \\ - MReg = 0, \end{aligned} \quad (25)$$

$$\begin{aligned} \theta'' + 2RePr\theta'f \\ + Tr \left[3\{\theta(T_d - 1) + 1\}^2(T_d - 1)(\theta')^2 \right] \\ + \left[\{\theta(T_d - 1) + 1\}^3(T_d - 1)\theta'' \right] \\ + Pr\beta\theta = 0, \end{aligned} \quad (26)$$

$$\frac{1}{ReSc}\phi'' + 2f\phi' - k_1\phi\phi^2 = 0, \quad (27)$$

$$\frac{\delta_1}{ReSc}\phi'' + 2f\phi' + k_1\phi\phi^2 = 0, \quad (28)$$

$$\left. \begin{aligned} f(0) = 0, f'(0) = A_1, f'(1) = A_2, g(0) = 1, \\ g(1) = \tau, \theta(0) = 1, \theta(1) = 0, \phi'(0) = k_2\phi(0), \\ \phi(1) = 1, \delta_1\phi(0) = -k_2\phi(0), \phi(1) = 0. \end{aligned} \right\} \quad (29)$$

The dimensionless quantities are defined as

$$\left. \begin{aligned} Re = \frac{\Omega_1 h^2}{\nu}, \varepsilon = \Omega_1 \beta_1, \tau = \frac{\Omega_2}{\Omega_1}, M = \frac{\delta B_0^2}{\rho \Omega_1}, \\ Pr = \frac{(\rho c_p)_f \nu}{k}, Sc = \frac{\nu}{D_B}, A_2 = \frac{c_2}{\Omega_1}, \\ \beta = \frac{Q_0 h^2}{(\rho c_p)_f \nu}, k_1 = \frac{k_c b_0^2}{\Omega_1}, k_2 = \frac{k_s h}{D_B}, \\ \delta_1 = \frac{D_C}{D_B}, Tr = \frac{16\delta^* T_2^3}{3kk^*}, \lambda_1 = \frac{g\alpha_1(T_1 - T_2)}{r\Omega_1^2}, \\ \lambda_2 = \frac{\alpha_2(T_1 - T_2)}{\alpha_1}, T_d = \frac{T_1}{T_2}, A_1 = \frac{c_1}{\Omega_1}. \end{aligned} \right\} \quad (30)$$

Note that Re indicates Reynolds number, ε material parameter, τ ratio of angular velocities, M Hartmann number (Magnetic parameter), Pr Prandtl number, Sc Schmidt number, A_1 and A_2 the scaled stretching parameters, β heat source parameter, k_1 and k_2 the strength of homogenous and heterogeneous reactions variables, δ_1 ratio of diffusion coefficient, Tr thermal radiation, λ_1 and λ_2 convection parameters and T_d the temperature parameter. Chemical species B and C have a comparable size of diffusion coefficient i.e. $\delta_1 = 1$. Thus one has

$$\phi(\eta) + \phi(\eta) = 1, \quad (31)$$

using equation (31) in (27) and (28), one obtains

$$\frac{1}{ReSc}\phi'' + 2f\phi' - k_1\phi(1 - \phi)^2 = 0. \quad (32)$$

Now velocity and temperature gradients can be define as

$$C_{f_r} = \frac{-2\tau_{w,r}}{\rho(u_w)^2}, C_{f_\theta} = \frac{-2\tau_{w,\theta}}{\rho(v_w)^2}, Nu_r = \frac{hq_w}{k(T_1 - T_2)}, \quad (33)$$

where $\tau_{w,r}$, $\tau_{w,\theta}$ represent shear stresses and q_w heat flux.

At right disk $\tau_{w,r}$, $\tau_{w,\theta}$ and q_w are defined as

$$\left. \begin{aligned} \tau_{w,r} = (\tau_{zr})_{z=0} &= \left(\mu \frac{\partial u}{\partial z} \right)_{z=0}, \\ \tau_{w,\theta} = (\tau_{z\theta})_{z=0} &= \left(\mu \frac{\partial v}{\partial z} \right)_{z=0}, \\ q_w &= \left[-k \left(\frac{\partial T}{\partial z} \right) + q_z \right]_{z=0} = \frac{-(T_1 - T_2)}{h} \\ &\quad \left[k + \frac{16\delta^* T_2^3}{3k^*} \{1 + (T_d - 1)\theta(0)\}^3 \right] \theta'(0). \end{aligned} \right\} \quad (34)$$

Thus skin friction and Nusselt number at right disk are obtained as

$$\left. \begin{aligned} C_{f_{r1}} &= \frac{-2}{(Re_r)A^2} [1 - 2n\varepsilon^2(f'(0))^2] f''(0), \\ C_{f_{\theta1}} &= \frac{-2}{(Re_r)} [1 - 2n\varepsilon^2(f'(0))^2] g'(0), \\ Nu_{r1} &= -[1 + Tr\{1 + (T_d - 1)\theta(0)\}^3] \theta'(0), \end{aligned} \right\} \quad (35)$$

where $Re_r = \frac{rh\Omega_1}{\nu}$ indicates local Reynolds number.

At left disk $\tau_{w,r}$, $\tau_{w,\theta}$ and q_w are addressed as

$$\left. \begin{aligned} \tau_{w,r} = (\tau_{zr})_{z=h} &= \left(\mu \frac{\partial u}{\partial z} \right)_{z=h}, \\ \tau_{w,\theta} = (\tau_{z\theta})_{z=h} &= \left(\mu \frac{\partial v}{\partial z} \right)_{z=h}, \\ q_w &= \left[-k \left(\frac{\partial T}{\partial z} \right) + q_z \right]_{z=h} = \frac{-(T_1 - T_2)}{h} \\ &\quad \left[k + \frac{16\delta^* T_2^3}{3k^*} \{1 + (T_d - 1)\theta(1)\}^3 \right] \theta'(1). \end{aligned} \right\} \quad (36)$$

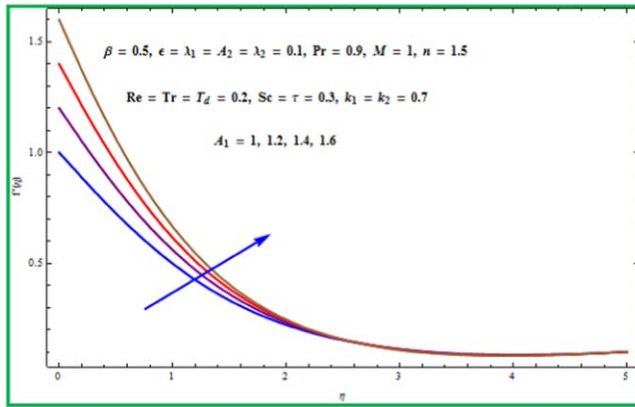
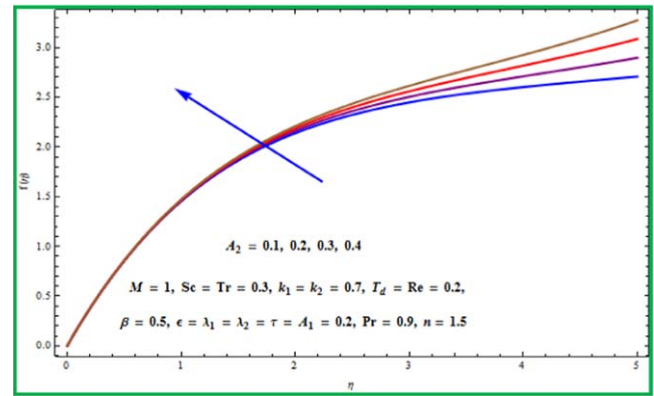
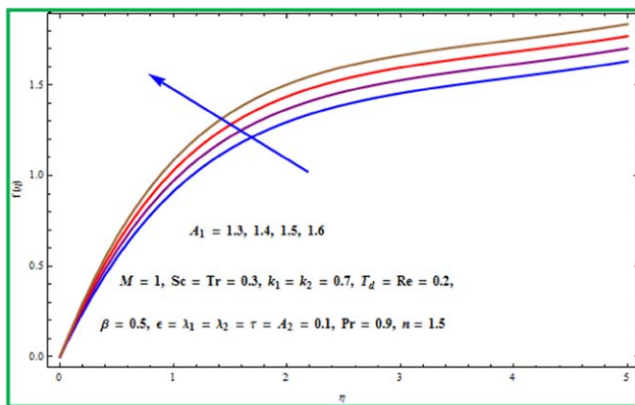
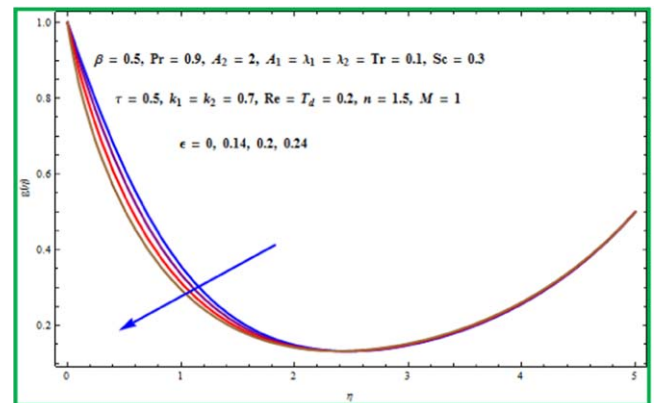
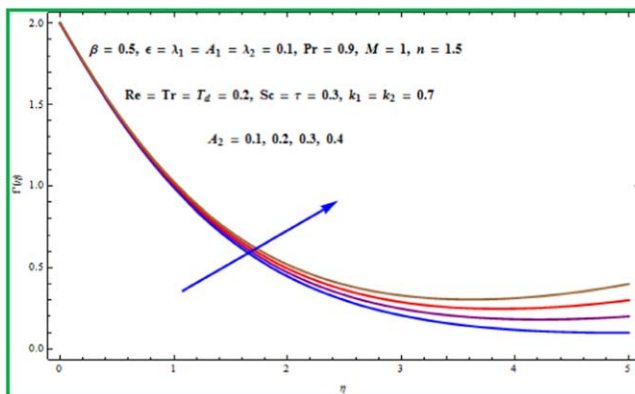
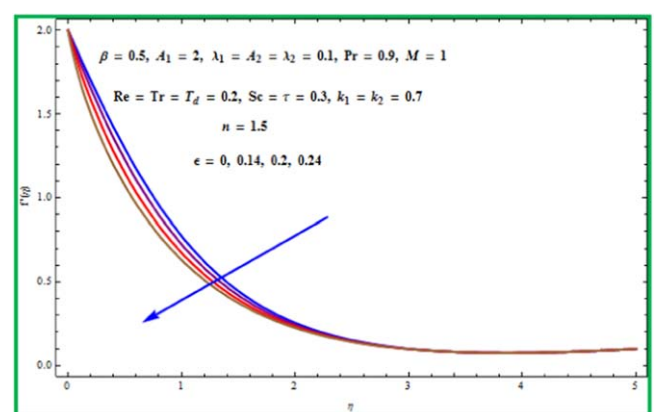
Thus skin friction and Nusselt number at left disk are obtained as

$$\left. \begin{aligned} C_{f_{r2}} &= \frac{-2}{(Re_r)A^2} [1 - 2n\varepsilon^2(f'(1))^2] f''(1), \\ C_{f_{\theta2}} &= \frac{-2}{(Re_r)} [1 - 2n\varepsilon^2(f'(1))^2] g'(1), \\ Nu_{r2} &= -[1 + Tr\{1 + (T_d - 1)\theta(1)\}^3] \theta'(1). \end{aligned} \right\} \quad (37)$$

4. Discussion

In this fragment, we have physically discussed and plotted the impact of pertinent flow variables on mass concentration, velocity fields (radial, axial and tangential) and temperature field. For this purpose, figures 2–25 are plotted. Shooting technique is used for the numerical solutions of the ordinary differential equations. The schematic flow diagram is presented in figure 1.

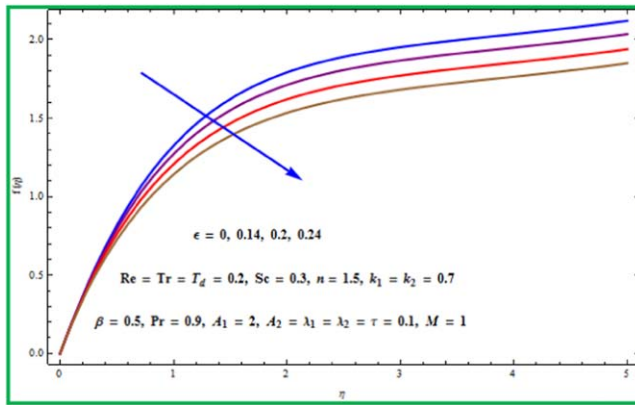
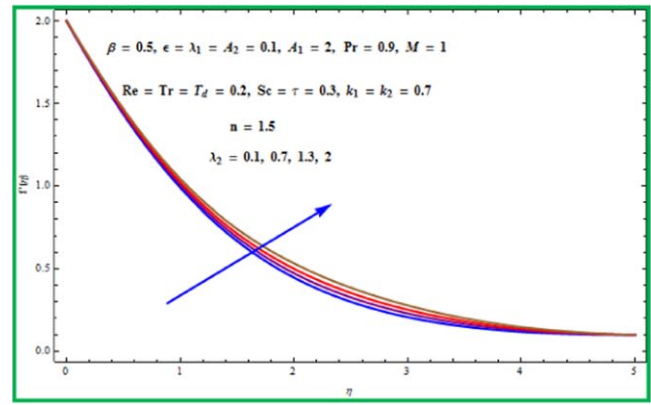
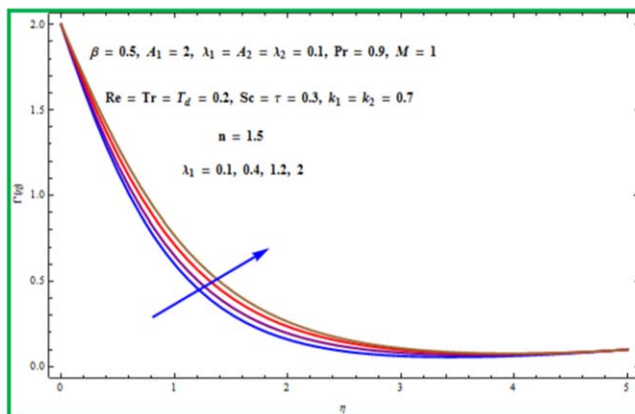
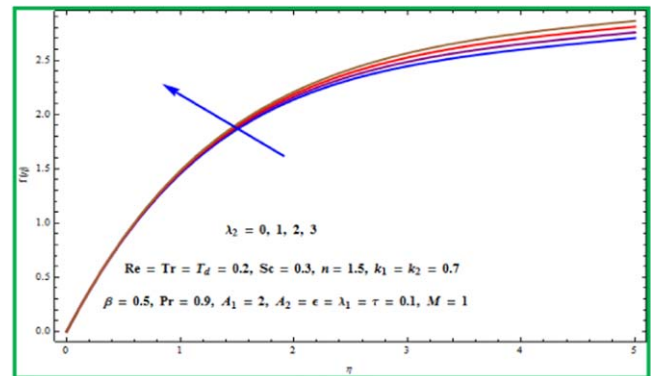
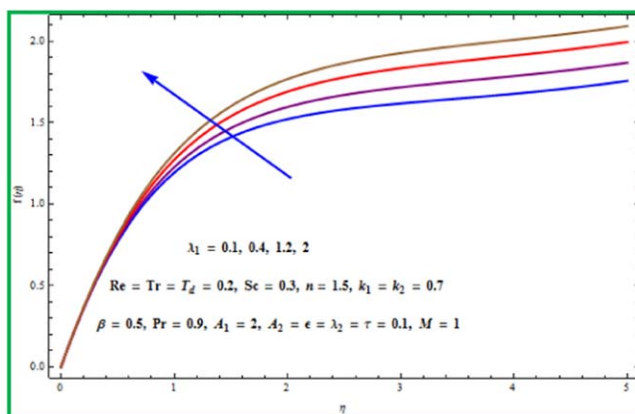
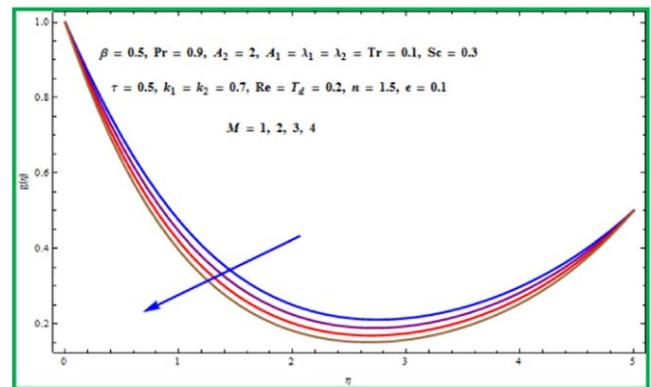
Table 1 is delineated to discuss the physical importance of skin friction coefficients at both lower and upper disks surface in the presence of various flow variables like

Figure 2. $f'(\eta)$ via A_1 .Figure 5. $f(\eta)$ via A_2 .Figure 3. $f(\eta)$ via A_1 .Figure 6. $g(\eta)$ via ϵ .Figure 4. $f'(\eta)$ via A_2 .Figure 7. $f'(\eta)$ via ϵ .

Reynolds number, Hartmann number, stretching parameters (A_1 , A_2) and mixed convection variables (λ_1 , λ_2). Here we have observed that the magnitude of skin friction coefficients ($C_{fr1}Re_r, C_{fr2}Re_r$) at both stretchable surfaces of disks increases versus higher values of Hartmann and Reynolds numbers. Physically, when we increase the range of Hartmann number, Lorentz force which is a resistive force enhances and as a result skin friction coefficients at both disks increase. Furthermore, opposite behavior of skin friction coefficients ($C_{fr1}Re_r, C_{fr2}Re_r$) is noticed at both disks for higher values of stretching parameters. At the surface of lower disk, the magnitude of skin friction increases through higher values of

stretching variable (A_1) and decreases at the surface of upper disk for larger (A_2). From physical point of view, when we enhance the range of stretching parameter (A_1), more disturbance is occurred to the flow of fluid particles and thus skin friction rate increases. Similar case is noticed at upper disk for higher estimations of stretching variable (A_2). Same impact is noticed at both upper and lower disks in the presence of larger mixed convection variables (λ_1 , λ_2).

Table 2 is inserted for the impact of skin friction coefficient in tangential direction versus different values of pertinent variables like stretching variables (A_1 , A_2), Hartmann

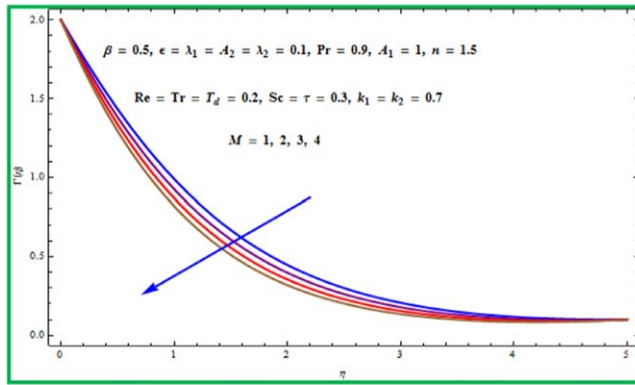
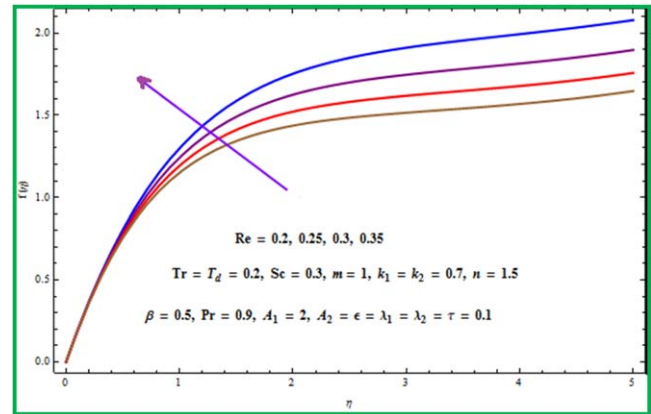
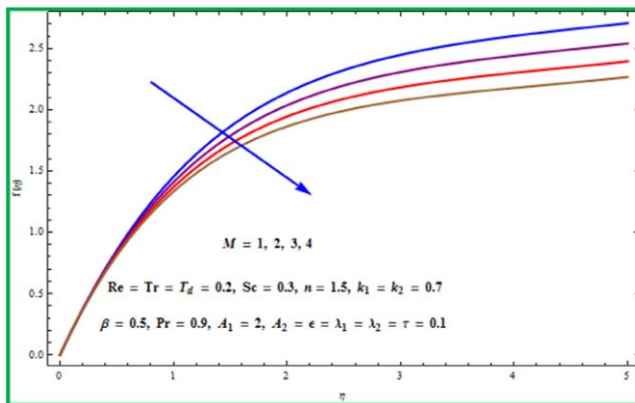
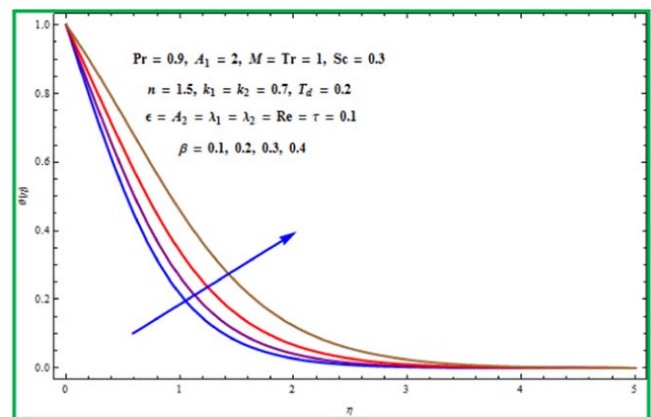
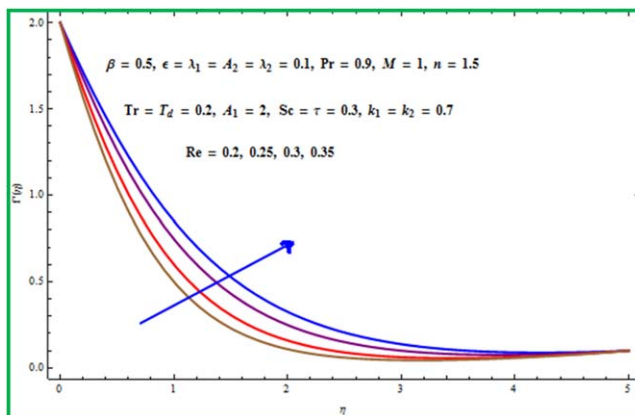
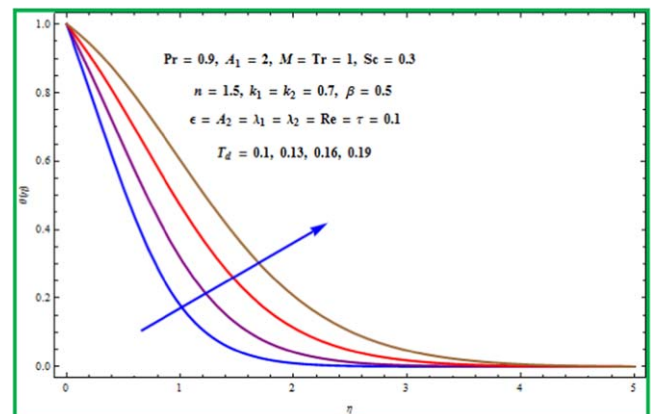
Figure 8. $f'(\eta)$ via ϵ .Figure 11. $f'(\eta)$ via λ_2 .Figure 9. $f'(\eta)$ via λ_1 .Figure 12. $f(\eta)$ via λ_2 .Figure 10. $f(\eta)$ via λ_1 .Figure 13. $g(\eta)$ via M .

number and ratio of angular velocities parameter. Clearly, it is noticed that the magnitude of skin friction coefficients at both stretchable surfaces of lower and upper disks increases through rising values of Hartmann number and stretching variables. But contrast impact at both lower and upper disks is noticed versus higher values of angular velocities ratio parameters. For higher values of angular velocities ratio parameter, the magnitude of skin friction in tangential direction decreases while increases at the surface of upper disk. Physically, when ratio of angular velocities parameter upsurges the angular rotation rate at lower disk decreases due to which

magnitude of skin friction coefficient decreases at lower disk as well as upper disk.

Table 3 is illustrated to present the behavior of Nusselt numbers (Nu_{r1} , Nu_{r2}) on both lower and upper disk surfaces through various parameters like Prandtl number, radiative parameter, temperatures ratio parameter and heat source/sink parameter. Clearly, it is noticed from table 3 that magnitude of heat transfer rate enhances for rising values of Prandtl number and temperature ratio parameter at both disks. But contrast impact is noticed for higher values of radiative parameter and heat generation parameter.

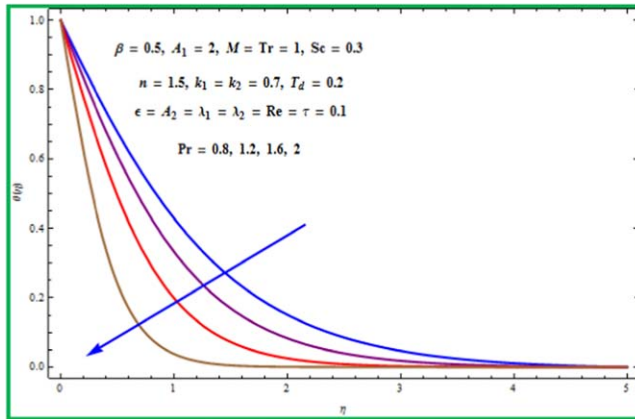
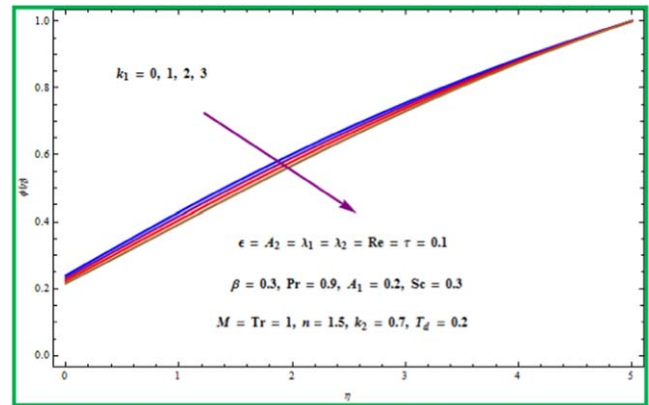
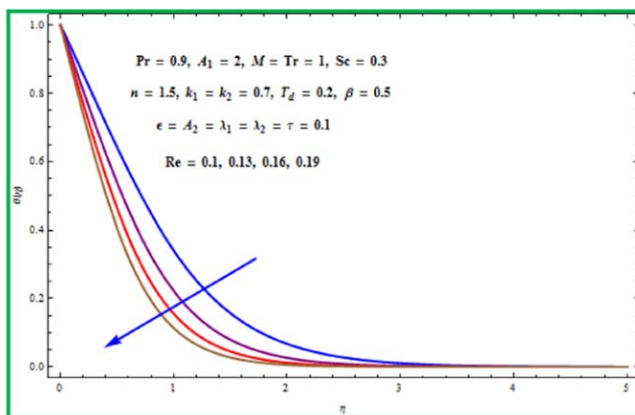
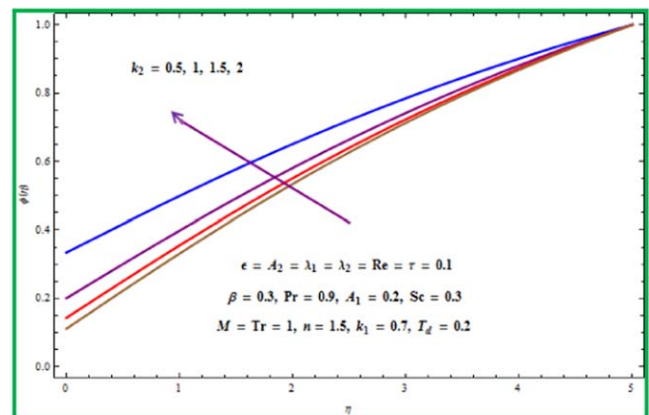
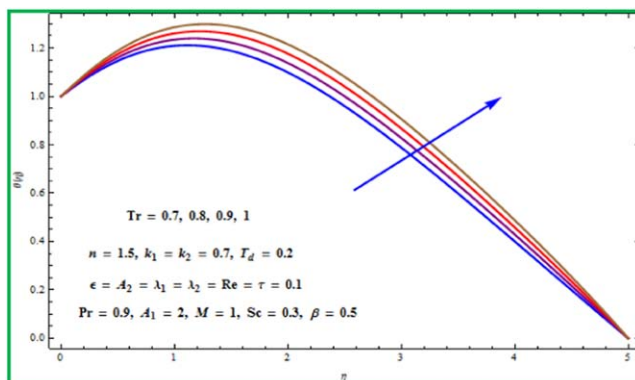
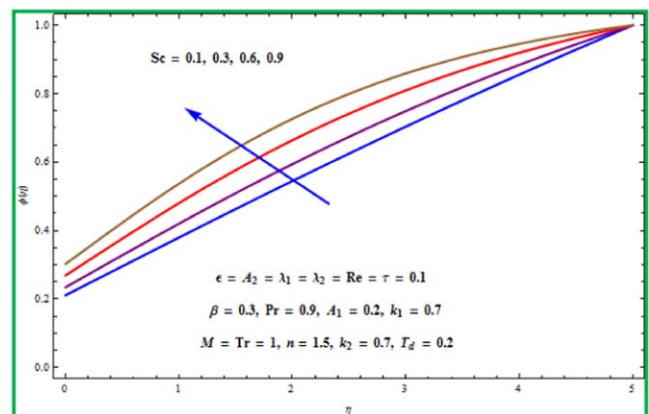
Characteristics of Reynolds number, material variable, ratio of angular velocities, Hartmann number, Prandtl

Figure 14. $f'(\eta)$ via M .Figure 17. $f(\eta)$ via Re .Figure 15. $f(\eta)$ via M .Figure 18. $\theta(\eta)$ via β .Figure 16. $f'(\eta)$ via Re .Figure 19. $\theta(\eta)$ via T_d .

number, thermal mixed convective parameters, heat source/sink parameter, stretching parameters, radiative parameter, homogeneous and heterogeneous reaction parameters, temperature ratio parameter and Schmidt number on mass concentration, temperature and velocity fields are discussed and presented in this section through plots. Figures 2–17 are explored to discussed the salient characteristics of $A_1, A_2, \epsilon, \lambda_1, \lambda_2, M, Re, Pr$ and Tr on velocity components i.e. (radial, axial, tangential). Figures 2–5 display the variation of velocity components for larger stretching variables. Physically, when we enhance the range of stretching parameters (A_1, A_2), stretching rate enhances due to which more

disturbance occurs in the material. The fluid particles will move more quickly which increases the velocity.

The characteristics of material variable on velocity components i.e. ($f'(\eta), f(\eta), g(\eta)$) are described in figures 6–8. Clearly, it is observed that velocity components decrease versus higher values of material parameter. Mathematically, the material parameter has a direct relation with B , which is associated with viscosity. Therefore, when we increase the range of material parameter, the viscosity of fluid

Figure 20. $\theta(\eta)$ via Pr .Figure 23. $\phi(\eta)$ via k_1 .Figure 21. $\theta(\eta)$ via Re .Figure 24. $\phi(\eta)$ via k_2 .Figure 22. $\theta(\eta)$ via Tr .Figure 25. $\phi(\eta)$ via Sc .

increases which produces resistance to the fluid particles. That is why velocity components decrease.

Figures 9–12 are sketched to show the impacts of thermal mixed convective parameters on the velocity components i.e. radial and axial velocities. Here velocity components increase versus higher values of thermal mixed convective parameters. Mathematically, the thermal mixed convective variables have direct relation with thermal expansion coefficients (α_1 , α_2). Physically, thermal expansion coefficient is a measure of change in length of a material in response to a change in its temperature. Thermal expansion coefficient is the property of

matter to change its area, shape and volume in response to a change in thermal field or temperature. Since temperature is a monotonic function of average molecular kinetic energy of a material or substance, so when a material is heated, the kinetic energy of the particles enhances. Therefore, the molecules of the material begin vibrating more rapidly. Therefore for rising values of thermal mixed convective parameters, the thermal expansion coefficient rate increases due to which the particles or molecules move more rapidly. That is why the velocity components increase versus these parameters.

Table 1. Numerical simulation for $C_{fr1}Re_r$ and $C_{fr2}Re_r$.

Re	M	A_1	A_2	λ_1	λ_2	$C_{fr1}Re_r$	$C_{fr2}Re_r$
0.1	0.2	0.8	0.7	0.1	0.5	0.745 705	−0.860 743
0.4						0.741 314	−0.852 365
0.5						0.807 818	−0.876 896
0.6						0.860 642	−0.893 3440
	0.3					0.833 605	−0.884 425
	0.4					0.922 945	−0.917 203
		0.8				0.741 314	−0.852 365
		0.9				0.830 175	−0.677 112
		1.0				0.876 624	−0.551 126
			0.7			0.741 314	−0.852 365
			0.8			0.706 372	−0.995 858
			0.9			0.671 488	−1.138 5560
				0.1		0.741 314	−0.852 365
				0.2		0.772 095	−0.851 671
				0.3		0.799 079	−0.851 264
					0.5	0.741 314	−0.852 365
					0.6	0.694 474	−0.853 463
					0.7	0.647 095	−0.854 569

Table 2. Numerical simulation for $C_{f\theta1}Re_r$ and $C_{f\theta2}Re_r$.

M	A_1	A_2	τ	$C_{f\theta1}Re_r$	$C_{f\theta2}Re_r$
0.2	0.8	0.7	0.5	1.556 48	−0.732 301
0.3				1.583 50	−0.734 612
0.4				1.621 93	−0.744 110
	0.8			1.544 82	−0.725 378
	0.9			1.600 96	−0.729 535
	1.0			1.654 00	−0.733 332
		0.7		1.544 82	−0.725 378
		0.8		1.551 46	−0.733 681
		0.9		1.557 86	−0.740 759
			0.5	1.534 82	−0.725 378
			0.6	1.533 68	−0.871 967
			0.7	1.522 76	−1.019 190

Table 3. Numerical simulation for Nu_{r1} and Nu_{r2} .

Pr	Tr	T_d	β	Nu_{r1}	Nu_{r2}
0.1	0.4	0.2	0.8	0.414 469	0.011 352 0700
0.2				0.304 723	0.018 525 800
0.3				1.946 270	−0.042 880 800
	0.4			0.414 469	0.013 520 700
	0.5			0.455 501	0.008 897 080
	0.6			0.507 917	0.004 985 570
		0.2		0.414 469	0.013 520 700
		0.3		0.416 956	0.015 894 100
		0.4		0.420 221	0.018 515 700
			0.8	0.414 469	0.013 520 700
			0.9	0.401 664	0.014 052 600
			1.0	0.388 618	0.014 608 700

Figures 13–15 are delineated for the salient aspects of Hartmann number on the velocity components i.e. radial, tangential and axial components. Mathematically, a Hartmann number is the ratio of electromagnetic force to the viscous

force which was introduced by Hartmann. It is a dimensionless number which gives a measure of relative importance of resistive forces from magnetic induction and viscous forces in fluid flow. The Lorentz force (which is a resistive force) increases versus higher values of Hartmann number and as a result velocity of fluid particles decreases.

Figures 16–17 highlight the physical importance of Reynolds number Re on velocity components i.e. radial, axial and tangential velocities. Mathematically, Reynolds number is the ratio of angular rotation and fluid viscosity. From these figures, it is noticed that the axial and radial velocity components increase versus higher values of Reynolds number. Physically, when we increase the range of Reynolds number, the viscosity of fluid diminishes and as a result velocity increases.

Figures 18–22 describe the characteristics of various pertinent variables like heat source/sink parameter, Reynolds number, radiation parameter, Prandtl number and temperatures ratio parameter on thermal field.

Figure 18 captures the impact of heat source/sink parameter on thermal field. Here thermal field is an increasing function of heat source/sink parameter. There are three cases for heat source/sink parameter (i) when $\beta > 0$ is called heat source parameter and (ii) when $\beta < 0$ is called heat sink parameter and when $\beta = 0$ there is no heat source/sink. In the current situation we only study the impact of heat source parameter on thermal field. Physically, when heat source parameter increase, more heat is produced in the working fluid or material due to which temperature field increases.

Figure 19 captures the behavior of temperatures ratio parameter on thermal field. Mathematically, temperature ratio parameter is the ratio of two different temperatures i.e. T_1 and T_2 , where T_1 is the temperature of lower disk and T_2 is the temperature of upper disk. When we increase the range of temperature ratio parameter, temperature at the lower disk increases. Here we have plot the graph for higher values of temperature ratio parameter at lower disk.

Thermal field versus higher values of Prandtl number is sketched in figure 20. Mathematically, Prandtl number is dimensionless number showing the ratio of momentum diffusivity (kinematic viscosity) to thermal diffusivity. The Prandtl number in the fluid flow is used for the identified the boundary layer. For higher values for Prandtl number the momentum diffusivity increases and thus thermal field decreases. From figure 20, it is noticed that lower (Pr) fluids or liquids having larger thermal conductivities endorsing faster diffusion of heat in thicker thermal layer structure related to higher (Pr) fluids or liquids in thinner layer region.

Figure 21 is plotted for the variation of higher values of Reynolds number on thermal field. Mathematically, Reynolds number is an essential dimensionless quantity in fluid flow utilized to predict flow patterns in different situations. For higher values of Reynolds number the viscosity of fluid decreases due to which resistive forces decay. Thus temperature decreases. Physically, when Reynolds number is small then the flow is laminar and when the Reynolds number is higher then the flow is turbulent.

Temperature field versus radiative parameter is highlighted in figure 22. Here thermal field is an increasing function of radiative parameter. Physically, for higher estimations of radiative parameter more heat is produced inside the working fluid due to which the kinetic energy increases. That is why thermal field is increased.

Figures 23–25 capture the influence of homogeneous reaction parameter, Schmidt number and heterogeneous reaction parameter on mass concentration field. Figures 23–24 are sketched to present the impact of homogeneous and heterogeneous reactions variables on mass concentration fields. Here concentration field decreases versus homogeneous reaction parameter and increases versus heterogeneous reaction variable. Physically, when we increase the range of homogeneous reaction parameter, the rate constants k_c enhances due to which reactants are consumed (see figure 23). Also, for higher values of heterogeneous reaction variable, diffusion coefficient diminishes due to which less diffused particles upsurge the mass concentration (see figure 24).

Figure 25 portrays the salient aspects of Schmidt number on concentration field. Clearly, it is observed that concentration field upsurgers via larger values of Schmidt number. Mathematically, Schmidt number is the ratio of momentum diffusivity (kinematic viscosity) and mass diffusivity. Physically, Schmidt number is utilized to describe liquid flows in which there are concurrent mass and momentum diffusion convection processes. Furthermore, Schmidt number also describes the mass momentum transport. Therefore, for higher Schmidt number the momentum diffusivity increases due to which mass diffusivity decreases and consequently concentration field increases.

5. Conclusion

Here we have examined the effects of homogeneous–heterogeneous reactions, MHD, nonlinear mixed convection, heat source/sink, nonlinear radiative heat flux in the flow of Sutterby fluid confined between two coaxially rotating disks. The key points of the studied problem are:

- Radial velocity is increased by A_1 , A_2 , λ_1 and λ_2 while it reduces with M , n and Re .
- Tangential velocity boosts via τ while it decreases through ϵ , M , n and Re .
- Elevation in A_1 , A_2 , λ_1 and λ_2 corresponds to higher axial velocity however it reduces with ϵ , M , n and Re .
- Temperature profile enhances for larger values of β , T_d and Tr however it decays through $3Pr$ and Re .
- Magnitudes of radial and tangential skin frictions at right disk are augmented for higher Re , M and A_1 they decrease with n and ϵ .
- Magnitudes of radial and tangential skin frictions at left disk are enhanced through Re , M and A_2 while decay with n , ϵ and λ_1 .
- Temperature gradient at right disk boosts via Re , Tr and T_d however it reduces with Pr , β and n .

- Temperature gradient at left disk enhances with Pr , T_d , β and n while it decays through Tr and Re .

ORCID iDs

M Ijaz Khan  <https://orcid.org/0000-0002-9041-3292>

Salman Ahmad  <https://orcid.org/0000-0002-7353-9600>

References

- [1] Karman T V 1921 Uber laminare und turbulente reibung *J. Appl. Math. Mech.* **1** 233–52
- [2] Kumar S K, Tacher W I and Watson L T 1989 Magnetohydrodynamic flow between a solid rotating disk and a porous stationary disk *Appl. Math. Model.* **13** 494–500
- [3] Turkyilmazoglu M 2014 Nanofluid flow and heat transfer due to a rotating disk *Comput. Fluid* **94** 139–46
- [4] Hayat T, Javed M, Imtiaz M and Alsaedi A 2017 Convective flow of Jeffrey nanofluid due to two stretchable rotating disks *J. Mol. Liq.* **240** 291–302
- [5] Sheikholeslami M, Hatami M and Ganji D D 2015 Numerical investigation of nanofluid spraying on an inclined rotating disk for cooling process *J. Mol. Liq.* **211** 577–83
- [6] Reddy P S, Sreedevi P and Chamkha A J 2017 MHD boundary layer flow, heat and mass transfer analysis over a rotating disk through porous medium saturated by Cu-water and Ag-water nanofluid with chemical reaction *Powder Tech.* **307** 46–55
- [7] Imtiaz M, Hayat T, Alsaedi A and Asghar S 2017 Slip flow by a variable thickness rotating disk subject to magnetohydrodynamics *Results Phys.* **7** 503–9
- [8] Doh D H and Muthamilselvan M 2017 Thermophoretic particle deposition on magnetohydrodynamic flow of micropolar fluid due to a rotating disk *Int. J. Mech. Sci.* **130** 350–9
- [9] Mustafa M 2017 MHD nanofluid flow over a rotating disk with partial slip effects: Buongiorno model *Int. J. Heat Mass Transfer* **108** 1910–6
- [10] Hayat T, Khan M I, Alsaedi A and Khan M I 2017 Joule heating and viscous dissipation in flow of nanomaterial by a rotating disk *Int. Commun. Heat Mass Transfer* **89** 190–7
- [11] Merkin J H 1996 A model for isothermal homogeneous–heterogeneous reactions in boundary layer flow *Math. Comput. Model.* **24** 125–36
- [12] Khan W A and Pop I 2010 Flow near the two-dimensional stagnation-point on an infinite permeable wall with a homogeneous–heterogeneous reaction *Commun. Nonlinear Sci. Numer. Simul.* **15** 3435–43
- [13] Hayat T, Khan M I, Farooq M, Yasmeen T and Alsaedi A 2016 Stagnation point flow with Cattaneo–Christov heat flux and homogeneous–heterogeneous reactions *J. Mol. Liq.* **220** 49–55
- [14] Khan M I, Waqas M, Hayat T and Alsaedi A 2017 A comparative study of Casson fluid with homogeneous–heterogeneous reactions *J. Colloid Interface Sci.* **498** 85–90
- [15] Arslan I and Balcioglu I A 1999 Degradation of commercial reactive dyestuffs by heterogenous and homogenous advanced oxidation processes: a comparative study *Dyes Pigments* **43** 95–108
- [16] Qayyum S, Khan M I, Hayat T and Alsaedi A 2016 A framework for nonlinear thermal radiation and homogeneous–heterogeneous reactions flow based on silver-water and copper-water nanoparticles: a numerical model for probable error *Results Phys.* **7** 1907–14

- [17] Tanveer A, Hayat T, Alsaedi A and Ahmad B 2017 Mixed convective peristaltic flow of Sisko fluid in curved channel with homogeneous–heterogeneous reaction effects *J. Mol. Liq.* **233** 131–8
- [18] Hayat T, Qayyum S, Alsaedi A and Waqas M 2016 Simultaneous influences of mixed convection and nonlinear thermal radiation in stagnation point flow of Oldroyd-B fluid towards an unsteady convectively heated stretched surface *J. Mol. Liq.* **224** 811–7
- [19] Rehman K U, Malik A A, Malik M Y and Saba N U 2017 Mutual effects of thermal radiations and thermal stratification on tangent hyperbolic fluid flow yields by both cylindrical and flat surfaces *Case Stud. Therm. Eng.* **10** 244–54
- [20] Hayat T, Qayyum S, Imtiaz M and Alsaedi A 2016 Comparative study of silver and copper water nanofluids with mixed convection and nonlinear thermal radiation *Int. J. Heat Mass Transfer* **102** 723–32
- [21] Ramzan M, Bilal M and Chung J D 2017 Effects of thermal and solutal stratification on Jeffrey magneto-nanofluid along an inclined stretching cylinder with thermal radiation and heat generation/absorption *Int. J. Mech. Sci.* **131–132** 317–24
- [22] Waqas M, Alsaedi A, Shehzad S A, Hayat T and Asghar S 2017 Mixed convective stagnation point flow of Carreau fluid with variable properties *J. Braz. Soc. Mech. Sci. Eng.* **39** 3005–17
- [23] Khan M, Irfan M and Khan W A 2017 Impact of nonlinear thermal radiation and gyrotactic microorganisms on the magneto-Burgers nanofluid *Int. J. Mech. Sci.* **130** 375–82
- [24] Waqas M, Khan M I, Hayat T and Alsaedi A 2017 Numerical simulation for magneto Carreau nanofluid model with thermal radiation: a revised model *Comput. Methods Appl. Mech. Eng.* **324** 640–53
- [25] Hayat T, Khan M I, Alsaedi A and Waqas M 2017 Mechanism of chemical aspect in ferromagnetic flow of second grade liquid *Results Phys.* **7** 4162–7
- [26] Hayat T, Ahmad S, Khan M I and Alsaedi A 2017 Non-darcy forchheimer flow of ferromagnetic second grade fluid *Results Phys.* **7** 3419–24
- [27] Hayat T, Qayyum S, Khan M I and Alsaedi A 2018 Entropy generation in magnetohydrodynamic radiative flow due to rotating disk in presence of viscous dissipation and Joule heating *Phys. Fluids* **30** 017101
- [28] Khan M I, Rashid M, Hayat T, Khan N B and Alsaedi A 2019 Physical aspects of Darcy–Forchheimer bidirectional flow in carbon nanotubes (SWCNTs and MWCNTs) *Int. J. Numer. Methods Heat Fluid Flow* **29** 2032–56
- [29] Khan M I, Yasmeen T, Khan M I, Farooq M and Wakeel M 2016 Research progress in the development of natural gas as fuel for road vehicles: a bibliographic review (1991–2016) *Renew. Sustain. Energy Rev.* **66** 702–41
- [30] Khan M W A, Khan M I, Hayat T and Alsaedi A 2018 Entropy generation minimization (EGM) of nanofluid flow by a thin moving needle with nonlinear thermal radiation *Physica B* **534** 113–9
- [31] Khan M I, Khan S A, Hayat T, Javed M F and Alsaedi A 2019 Entropy generation in radiative flow of Ree–Eyring fluid due to two rotating disks *Int. J. Numer. Methods Heat Fluid Flow* **29** 2057–79
- [32] Hayat T, Khan M I, Qayyum S, Alsaedi A and Khan M I 2018 New thermodynamics of entropy generation minimization with nonlinear thermal radiation and nanomaterials *Phys. Lett. A* **382** 749–60
- [33] Khan M I, Hayat T, Waqas M, Khan M I and Alsaedi A 2018 Entropy generation minimization (EGM) in nonlinear mixed convective flow of nanomaterial with Joule heating and slip condition *J. Mol. Liq.* **256** 108–20
- [34] Mahdy A and Chamkha A J 2018 Unsteady MHD boundary layer flow of tangent hyperbolic two-phase nanofluid of moving stretched porous wedge *Int. J. Numer. Methods Heat Fluid Flow* **28** 2567–80
- [35] Khan M I, Sumaira S, Hayat T, Waqas M, Khan M I and Alsaedi A 2018 Entropy generation minimization and binary chemical reaction with Arrhenius activation energy in MHD radiative flow of nanomaterial *J. Mol. Liq.* **259** 274–83
- [36] Khan M I, Ullah S, Hayat T, Khan M I and Alsaedi A 2016 Entropy generation minimization (EGM) for convection nanomaterial flow with nonlinear radiative heat flux *J. Mol. Liq.* **260** 279–91
- [37] Govindaraju M, Ganesh N V, Ganga B and Hakeem A K A 2015 Entropy generation analysis of magneto hydrodynamic flow of a nanofluid over a stretching sheet *J. Egypt. Math. Soc.* **23** 429–34
- [38] Qayyum S, Hayat T, Khan M I, Khan M I and Alsaedi A 2018 Optimization of entropy generation and dissipative nonlinear radiative Von Karman’s swirling flow with Soret and Dufour effects *J. Mol. Liq.* **262** 261–74
- [39] Khan M I, Qayyum S, Hayat T, Khan M I, Alsaedi A and Khan T A 2018 Entropy generation in radiative motion of tangent hyperbolic nanofluid in presence of activation energy and nonlinear mixed convection *Phys. Lett. A* **382** 2017–26
- [40] Haq F, Rahman M U, Khan M I and Alsaedi A 2019 Transportation of activation energy in development of binary chemical reaction to investigate the behavior of Oldroyd-B fluid with nanomaterial *Phys. Scr.* **94** 105010
- [41] Khan M I, Qayyum S, Hayat T, Alsaedi A and Khan M I 2018 Investigation of Sisko fluid through entropy generation *J. Mol. Liq.* **257** 155–63
- [42] Hayat T, Khan M I, Qayyum S, Khan M I and Alsaedi A 2018 Entropy generation for flow of Sisko fluid due to rotating disk *J. Mol. Liq.* **264** 375–85
- [43] Hayat T, Khan S A, Khan M I and Alsaedi A 2019 Optimizing the theoretical analysis of entropy generation in flow of second grade nanofluid *Phys. Scr.* **94** 085001
- [44] Khan M I, Hayat T, Alsaedi A, Qayyum S and Tamoore M 2018 Entropy optimization and quartic autocatalysis in MHD chemically reactive stagnation point flow of Sisko nanomaterial *Int. J. Heat Mass Transfer* **127** 829–37
- [45] Hayat T, Khan M I, Farooq M, Alsaedi A, Waqas M and Yasmeen T 2016 Impact of Cattaneo–Christov heat flux model in flow of variable thermal conductivity fluid over a variable thickened surface *Int. J. Heat Mass Transfer* **99** 702–10
- [46] Khan M I, Khan M W A, Hayat T and Alsaedi A 2019 Dissipative flow of hybrid nanomaterial with entropy optimization *Mater. Res. Express* **6** 085003
- [47] Khan M I, Hayat T, Khan M I and Alsaedi A 2018 Activation energy impact in nonlinear radiative stagnation point flow of cross nanofluid *Int. Commun. Heat Mass Transfer* **91** 216–24
- [48] Kamal F, Zaimi K, Ishak A and Pop I 2018 Stability analysis on the stagnation-point flow and heat transfer over a permeable stretching/shrinking sheet with heat source effect *Int. J. Numer. Methods Heat Fluid Flow* **28** 2650–63
- [49] Qayyum S, Khan M I, Hayat T and Alsaedi A 2017 A framework for nonlinear thermal radiation and homogeneous–heterogeneous reactions flow based on silver-water and copper-water nanoparticles: a numerical model for probable error *Results Phys.* **7** 1907–14
- [50] Hayat T, Khan M I, Waqas M, Khan M I and Alsaedi A 2017 Radiative flow of micropolar nanofluid accounting thermophoresis and Brownian moment *Int. J. Hydrog. Energy* **42** 16821–33

- [51] Nazeer M, Ali N and Javed T 2018 Effects of moving wall on the flow of micropolar fluid inside a right angle triangular cavity *Int. J. Numer. Methods Heat Fluid Flow* **28** 2404–22
- [52] Hayat T, Khan M I, Farooq M, Yasmeen T and Alsaedi A 2016 Water-carbon nanofluid flow with variable heat flux by a thin needle *J. Mol. Liq.* **224** 786–91
- [53] Mahanthesh B, Gireesha B J, Archana M, Hayat T and Alsaedi A 2018 Variable viscosity effects on third-grade liquid flow in post-treatment analysis of wire coating in the presence of nanoparticles *Int. J. Numer. Methods Heat Fluid Flow* **28** 2423–41
- [54] Khan M I, Waqas M, Hayat T, Khan M I and Alsaedi A 2017 Behavior of stratification phenomenon in flow of Maxwell nanomaterial with motile gyrotactic microorganisms in the presence of magnetic field *Int. J. Mech. Sci.* **132** 426–34
- [55] Teleszewski T J and Sorko S A 2018 Effect of viscous dissipation on forced convection for laminar flow through a straight regular polygonal duct using BEM method *Int. J. Numer. Methods Heat Fluid Flow* **28** 220–38
- [56] Khan M I, Hayat T, Waqas M, Khan M I and Alsaedi A 2017 Impact of heat generation/absorption and homogeneous–heterogeneous reactions on flow of Maxwell fluid *J. Mol. Liq.* **233** 465–70
- [57] Hdhiri N and Beya B B 2018 Numerical study of laminar mixed convection flow in a lid-driven square cavity filled with porous media: Darcy–Brinkman–Forchheimer and Darcy–Brinkman models *Int. J. Numer. Methods Heat Fluid Flow* **28** 857–77
- [58] Hayat T, Qayyum S, Khan M I and Alsaedi A 2018 Entropy generation in magnetohydrodynamic radiative flow due to rotating disk in presence of viscous dissipation and Joule heating *Phys. Fluids* **30** 01710
- [59] Hammami F, Cheikh N B, Beya B B and Souayah B 2018 Combined effects of the velocity and the aspect ratios on the bifurcation phenomena in a two-sided lid-driven cavity flow *Int. J. Numer. Methods Heat Fluid Flow* **28** 943–62
- [60] Waqas M, Khan M I, Hayat T, Alsaedi A and Khan M I 2017 On Cattaneo–Christov double diffusion impact for temperature-dependent conductivity of Powell–Eyring liquid *Chin. J. Phys.* **55** 729–73
- [61] Brewster M Q 1992 *Thermal Radiative Transfer Properties* (Canada: Wiley)
- [62] Mahabaleswar U S, Nagaraju K R, Kumar P N V, Baleanu D and Lorenzini G 2017 An exact analytical solution of the unsteady magnetohydrodynamics nonlinear dynamics of laminar boundary layer due to an impulsively linear stretching sheet *Contin. Mech. Thermodyn.* **29** 559–67
- [63] Siddheshwar P G and Mahabaleswar U S 2005 Effects of radiation and heat source on MHD flow of a viscoelastic liquid and heat transfer over a stretching sheet *Int. J. Nonlinear Mech.* **40** 807–20